ISSN 1063-7761, Journal of Experimental and Theoretical Physics, 2018, Vol. 126, No. 4, pp. 523–534. © Pleiades Publishing, Inc., 2018.
Original Russian Text © V.A. Orlov, R.Yu. Rudenko, A.V. Kobyakov, A.V. Lukyanenko, P.D. Kim, V.S. Prokopenko, I.N. Orlova, 2018, published in Zhurnal Eksperimental'noi i Teoreticheskoi Fiziki, 2018, Vol. 153, No. 4, pp. 627–640.

ORDER, DISORDER, AND PHASE TRANSITION IN CONDENSED SYSTEM

Magnetization Dynamics in Two-Dimensional Arrays of Square Microelements

V. A. Orlov[a,b,*], R. Yu. Rudenko[a,b], A. V. Kobyakov[a,b], A. V. Lukyanenko[a,b], P. D. Kim[a†], V. S. Prokopenko[c], and I. N. Orlova[c]

[a] *Kirensky Institute of Physics, Siberian Branch, Russian Academy of Sciences, Krasnoyarsk, 660036 Russia*
[b] *Siberian Federal University, Svobodnyi pr. 79, Krasnoyarsk, 660041 Russia*
[c] *Astaf'ev Krasnoyarsk State Pedagogical University, ul. Ady Lebedevoi 89, Krasnoyarsk, 660049 Russia*
**e-mail: orlhome@rambler.ru*

Received December 11, 2017

Abstract—The collective magnetization motion in an array of magnetostatically interacting ferromagnetic square elements is studied theoretically and experimentally. Dispersion laws are obtained for collective modes for some particular cases of the distribution of the topological charges π_T of magnetic vortices in particles. Resonance curves are plotted with allowance for dissipation for various values of π_T. An experimental investigation of the ferromagnetic resonance in a two-dimensional array of particles qualitatively supports the calculation results.

DOI: 10.1134/S1063776118040118

1. INTRODUCTION

Interest in studying nano- and microobjects (nano- and microdots) is related to the prospects of using such materials in ultrahigh-density data storage devices, spintronic devices, and microsurgery. The magnetic properties of individual nanodots and their arrays have important specific features. For example, one such element can hold two bits. One bit can be coded in the sign of polarity p of a magnetic vertex core, and the second bit, in the sign of chirality q. Under certain conditions, the equilibrium magnetization distribution in nanodots is known to be a magnetic vortex with a core, which is a small region having a strongly nonuniform magnetization, at its center. The magnetization direction at the center of the core is perpendicular to the nanodot surface and is characterized by polarity $p = \pm 1$, conventionally "up" and "down". The average core radius can be estimated from the relation $\delta \approx \sqrt{A/K_{\text{eff}}}$, where A and K_{eff} are the exchange and surface anisotropy constants, respectively. δ for most soft magnetic materials is several tens of nanometers. Magnetization in a vortex can have a conventional clockwise or counterclockwise direction, which is characterized by the sign of parameter $q = \pm 1$.

The analytical description of the dynamic properties of nanodots is based on the Landau–Lifshitz–Gilbert equation and its modification proposed by Thiele [1]. The Thiele approach is as follows. In the presence of magnetization soliton heterogeneity, the equation of magnetization motion is rewritten in terms of collective variables, one of which is the coordinate of the center of the heterogeneity. In this form, Thiele's equation acquires a non-Newtonian form for the description of a magnetic vortex at a nanodot [2]. In an ac field, the core of a magnetic soliton is involved in complex motion under the action of a gyroforce [3–6]. It should be noted that the trajectory of core motion in nanospots with a nonspherical (elliptical) shape can differ substantially from a circular one, and the application of Thiele's equation is complicated.

Force microscopy is the main method for controlling the magnetic state in submicron particles [7–10]. To control polarity and chirality under resonance conditions, researchers use short spin-polarized current pulses (see, e.g., [11]) and field pulses [12–15], and gradient fields turn out to be effective in the arrays of square elements [16].

The element arrangement density in a matrix should be as high as possible in high-density data storage devices and spintronic devices. The interaction between the magnetic subsystems substantially affects the magnetization dynamics in such arrays of closely spaced magnets. As a rule, this interaction has a magnetostatic origin; however, an indirect exchange of conduction electrons [17] and a direct exchange can take place in the presence of magnetic "bridges" between neighboring elements [18]. Therefore, a spectrum of experimental and theoretical works has recently appeared to study the influence of an inter-

† Deceased.

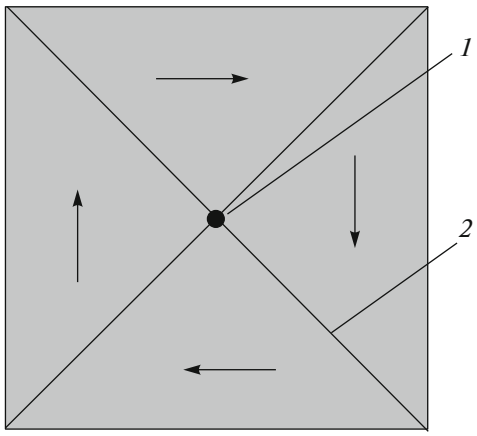

Fig. 1. Schematic diagram of the equilibrium magnetization structure in a square ferromagnet: (*1*) core and (*2*) domain wall.

particle interaction on the static and dynamic magnetic properties of arrays.

For theoretical calculations, researchers most often apply the model concepts where a magnetostatic interaction is set in the dipole approximation. For example, the authors of [19, 20] analytically calculated the laws of dispersion of one- and two-dimensional arrays with allowance for only the dipole interaction of the magnetic moments of cores. The law of dispersion was studied in [21] using the model of an array of circular elements with the same chirality, and this law was investigated in [9] by alternating both parameters. In both arrays with a large number of nano- and microdots and small sets [22–25], the removal of resonance frequency degeneracy due to the interaction between elements was predicted and discovered. In most works dealing with the collective modes in arrays, calculations were carried out without regard for dissipation and only for some possible combinations of polarities and chiralities. In this work, we try to close this gap for an array of square micron-sized (submicron) elements.

The behavior of a core in ac magnetic fields at a relatively low frequency (less than 1 GHz) is similar to the gyrotropic motion of a quasiparticle in the field of effective forces [26–31]. A structure of triangle domains separated by 90° walls of the Néel type forms in micron and submicron square magnets. The core of a vortex forms at the intersection of domain walls at the center of a square (Fig. 1). When the core moves from the center of a square, the action of demagnetizing fields causes an effective restoring force and a gyroforce, which is induced by spin precession in the effective field of a magnet. In this case, the motion of the core is similar to the Larmor gyration of a charged particle about the lines of a magnetic field. The gyration frequency is several hundred megahertzs, which is significantly lower than the domain wall oscillation frequency. It is interesting that both magnetization motion modes, namely, core gyration and domain wall oscillation, were experimentally detected in the arrays of square elements [32]. The substantial difference between the frequencies of these modes suggests that the presence of a domain structure insignificantly affects the character of the gyrotropic motion of a vortex core.

We write Thiele's equation in the form

$$\mathbf{G}\times\mathbf{v} - D\mathbf{v} - \nabla U = 0, \quad (1)$$

where $\mathbf{G}$ is the gyrovector, $\mathbf{v}$ is the velocity vector of the magnetic vortex core, D is the coefficient of effective viscous friction, and U is the effective potential core energy. The gyrovector can be represented as [11, 30, 33]

$$\mathbf{G} = \pi_T G_0(1 - ph)\mathbf{k},$$

where $\pi_T = pq$ is the topological charge of the magnetic vortex [34, 35], $G_0 = 2\pi M_s l/\gamma$, M_s is the saturation magnetization, $h = H_z/H_s$, $H_s \approx 10$ kOe is the saturation field along axis z, l is the element thickness, and γ is the gyromagnetic ratio. Axis z is perpendicular to the film surface and $\mathbf{k}$ is the unit vector along axis z. U is the core energy in the effective field of a square element. The effective field can include the terms caused by the Zeeman energy, the interparticle interaction energy, the stray field energy, and so on. From here on, we restrict ourselves to these factors,

$$U = U_p + U_{\text{dip}} + U_H, \quad (2)$$

where U_H is the core energy related to the interaction of the magnetic subsystem of the element and an applied magnetic field. U_{dip} describes the energy of the pair magnetostatic interaction between array elements. The interaction between the magnetic moments of the cores, which is relatively weak (because of the small core volume) [36] should be distinguished from the interaction between the magnetic moments of the remaining volume of squares. The former interaction exists irrespective of a vector coordinate. The latter interaction can be high and appears between induced magnetic moments solely due to the shift of a core from the center of a magnet. To estimate this shift, it is useful to apply the magnetic charge method in the rigid vortex model [37, 38]. Parameter U_p is the potential energy of the core, which increases when it shifts from an equilibrium position (center of spot). As a rule, an increase in this term is related to an increase in the demagnetizing fields. For an insignificant displacement of a core from its equilibrium position, we can write $U_p = \kappa\mathbf{r}^2$, where $\kappa = \kappa_0(1 - h^2)$ is the effective rigidity of the quasi-elastic force on the core (for circular elements, see [11, 30, 33]) and $\mathbf{r}$ is the radius vector of the center of the core that originates in the center of the square. The problem of an explicit dependence of parameter D on the parameters of magnetic elements is rather complex, and it is difficult to find an analytical expression. In this work, we use the estimates obtained in [39–42].

Despite a wide spectrum of works dealing with the magnetic properties of individual square submicron-sized magnets, the question of an explicit form of κ_0 is still open. As a rule, this problem is partly resolved by a numerical simulation of magnetization dynamics, since this approach does not need an analytical formula. The purpose of this work is to calculate magnetization oscillation spectra. Therefore, we first approximately compute the effective rigidity as a function of the magnet parameters.

2. EFFECTIVE CORE POTENTIAL IN A SQUARE MICROELEMENT

We now estimate the change in the potential magnetostatic energy when the core of a rigid vortex shifts from the center of a square nanodot (Fig. 2). When the core moves, magnetostatic charges appear on the lateral surface and interact with each other. Eight charge-alternating regions, which are indicated by curly brackets in Fig. 2, can be distinguished. We now calculate the energy of their pair interaction.

As an example, we consider the interaction of regions 1–2 in detail. An expression for the surface density of magnetic charges in region 1 has the form

$$\sigma_1 = M_s \sin\phi = M_s \frac{u}{\sqrt{(L/2-x)^2+u^2}}, \tag{3}$$

where L is the side of square. Similar formulas can be derived for other regions. Then, for the energy of interaction of small regions located at distances u and v from the vortex core, we can write

$$\begin{aligned} dE_{12} &= \frac{\mu_0 M_s^2 h^2}{4\pi}\frac{uvdudv}{u-v} \\ &\times\left\{\left[\left(\frac{L}{2}-x\right)^2+u^2\right]\left[\left(\frac{L}{2}-x\right)^2+v^2\right]\right\}^{-1/2} \\ &= \frac{\mu_0 M_s^2 h^2 L}{4\pi}\frac{u'v'du'dv'}{u'-v'} \\ &\times\left\{\left[\left(\frac{1}{2}-\frac{x}{L}\right)^2+u'^2\right]\left[\left(\frac{1}{2}-\frac{x}{L}\right)^2+v'^2\right]\right\}^{-1/2}, \end{aligned} \tag{4}$$

where μ_0 is the magnetic constant. From here on, we introduce dimensionless variables $u' = u/L$ and $v' = v/L$. For the interaction energy of regions on one face, we have

$$\begin{aligned} E_{12} &= \frac{\mu_0 M_s^2 h^2 L}{4\pi}\int\limits_{-\left(\frac{1}{2}+\frac{y}{L}\right)}^{\frac{1}{2}-\frac{y}{L}}\int\limits_{u'}^{\frac{1}{2}-\frac{y}{L}}\frac{u'v'du'dv'}{u'-v'} \\ &\times\left\{\left[\left(\frac{1}{2}-\frac{x}{L}\right)^2+u'^2\right]\left[\left(\frac{1}{2}-\frac{x}{L}\right)^2+v'^2\right]\right\}^{-1/2}. \end{aligned} \tag{5}$$

Similarly, we obtain expressions for the energies of interaction of the other three faces, E_{34}, E_{56}, and E_{78}.

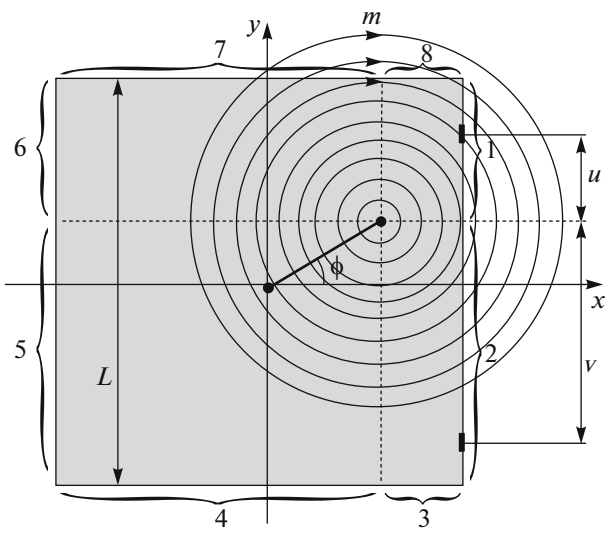

Fig. 2. Magnetization configuration of a shifted rigid vortex in a square nanodot (**m** is magnetization unit vector).

Moreover, we have to calculate the interaction energies of regions on different faces. For example, for the pair energy of neighboring faces 12–78, we can write

$$E_{12-78} = \frac{\mu_0 M_s^2 h^2 L}{4\pi} I\left(\frac{x}{L},\frac{y}{L}\right), \tag{6}$$

where

$$\begin{aligned} I\left(\frac{x}{L},\frac{y}{L}\right) &= \int\limits_{-\left(\frac{1}{2}-\frac{x}{L}\right)}^{\frac{1}{2}+\frac{x}{L}}\int\limits_{-\left(\frac{1}{2}+\frac{y}{L}\right)}^{\frac{1}{2}-\frac{y}{L}}\frac{y'v'du'dv'}{u'-v'} \\ &\times\left\{\left[\left(\frac{1}{2}-\frac{x}{L}\right)^2+u'^2\right]\left[\left(\frac{1}{2}-\frac{y}{L}\right)^2+v'^2\right]\right. \\ &\left.\times\left[\left(\frac{1}{2}-\frac{x}{L}+v'\right)^2\right]\left[\left(\frac{1}{2}-\frac{y}{L}-u'\right)^2\right]\right\}^{-1/2}. \end{aligned} \tag{7}$$

A similar calculation is performed for the remaining pairs of regions. The total energy of a square element is

$$\begin{aligned} W_b &= E_{12}+E_{34}+E_{56}+E_{78}+E_{12-34}+E_{12-56} \\ &+E_{12-78}+E_{34-56}+E_{34-78}+E_{56-78}. \end{aligned} \tag{8}$$

Figure 3 shows the results of a numerical calculation of the dimensionless part of energy (integrals). It is seen that, as the core travels a certain critical distance from the center of square, the restoring force disappears. The core freely moves toward the edge of the element and disappears. This effect does take place, but the rigid vortex model cannot give a reliable critical displacement. The further analysis is performed provided the displacement of the core from the center of square is small.

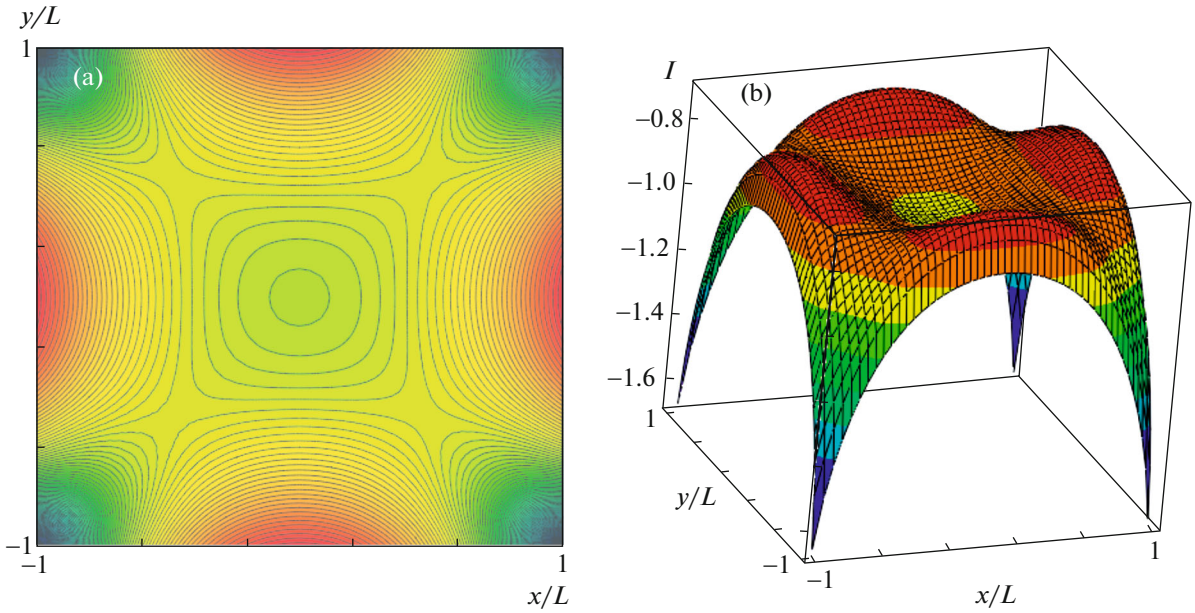

Fig. 3. (Color online) Profile of the dimensionless part of the potential energy (7) of a square element: (a) outline picture and (b) potential surface.

At a small core displacement, potential (8) is well approximated by the function

$$W_b = 5\frac{\mu_0 M_s^2 h^2 L}{\pi}\left[\left(\frac{x}{L}\right)^2 - \frac{1}{4}\right]\left[\left(\frac{y}{L}\right)^2 - \frac{1}{4}\right], \qquad (9)$$

and we can write

$$\kappa_0 \approx \frac{5\mu_0 M_s^2 h^2}{4\pi L} \qquad (10)$$

for the quasi-rigidity coefficient at small displacements. Figure 4 shows the qualitative (without regard for the type of substance) trajectory of a vortex core in potential (9) that was plotted using the results of a numerical solution of Eq. (1).

In the presence of a constant force component in the magnet plane, the vortex core moves from the center to a potential region with a lower quasi-rigidity coefficient, which follows from Eq. (9). The period of core revolution increases with the in-plane component of force. This finding explains the high sensitivity of resonance curves to the sample orientation with respect to a dc magnetic-field component [9]. Note that this effect is much weaker in circular nanodots, since the effective rigidity of the magnetic subsystem in circular magnets weakly depends on the core displacement. Thus, the motion of the core in a square magnet can be described in a linear approximation at the in-plane fields that are much lower than those allowed for circular elements.

3. NORMAL MODES OF COLLECTIVE CORE MOTION

We now consider a model to qualitatively understand the cause of splitting of ferromagnetic resonance (FMR) frequencies. Let us analyze a two-dimensional array of ferromagnetic square elements, the centers of which are spaced d apart. In this case, the coordinates of the centers of the elements are set as follows: $X_{n,m} = nd$ and $Y_{n,m} = md$ (Fig. 5).

The interaction as a function of the interparticle distance in the array was studied in a number of works. The authors of [43, 44] showed that the interaction energy is proportional to d^{-6} in the absence of an applied field. The mutual influence of the magnetic subsystems of a pair of elements causes the effect that is analogous to the polarization of gas molecules; therefore, the authors pointed to an analogy with the van der Waals forces. As was shown in [41], the energy of pair interaction is proportional to $d^{-3.6}$ in the presence of a magnetic field applied normal to the film surface. The reduction in the power can be explained if we take into account the relative weakness of the magnetostatic interaction as compared to the Zeeman energy in the fields that can substantially change effective parameters G and κ. When the applied fields increases, the quality of the dipole approximation used to describe the interaction energy becomes higher. Here, we restrict ourselves to the dipole approximation where energy is proportional to d^{-3}, which is admissible for an insignificant core displacement from an equilibrium position, a predominant perpendicular dc field component and a minor in-

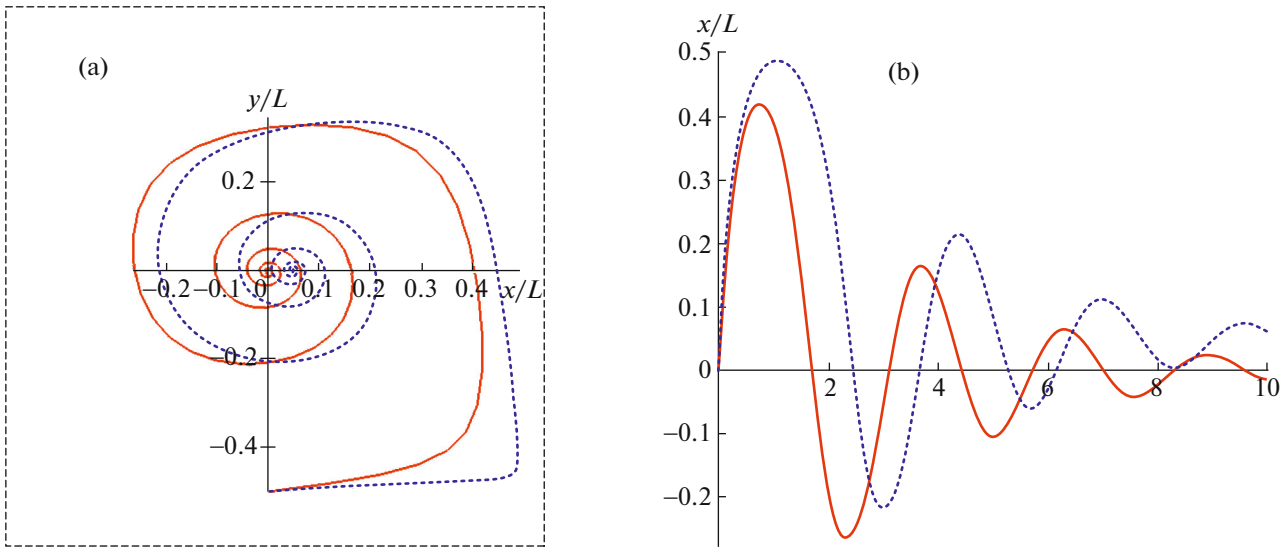

Fig. 4. (Color online) (a) Characteristic trajectories of the core of a magnetic vortex in a square microelement. (b) Time dependence of the core coordinate; the period of core revolution increases with the displacement from the center of the square. (dotted curves) Trajectories in the presence of a magnetic field in the square plane along axis y and (solid curves) trajectory in zero field.

plane ac field component, and the field created by the magnetization of the remaining array elements.

We now represent the terms from Eq. (2) as functions of the core coordinate. For the energy of the magnetostatic interaction of two elements spaced n horizontal periods and m vertical periods apart, we can write (Fig. 6)

$$W_{n,m} = \frac{\mu_0}{4\pi}\left[\frac{\mathbf{M}\cdot\mathbf{M}_{n,m}}{(n^2+m^2)^{3/2}d^3} - \frac{3(\mathbf{M}\cdot\mathbf{r}_{n,m})(\mathbf{M}_{n,m}\cdot\mathbf{r}_{n,m})}{(n^2+m^2)^{5/2}d^5}\right],$$

where $\mathbf{r}_{n,\,m}$ is the radius vector connecting the centers of the squares under study. Figure 6 shows the schematic diagram that can help one to understand how the magnitude and the orientation of magnetic moment $\mathbf{M}$ of an element depend on the core coordinate. Obviously, for the projections of the magnetic moment of an element onto the coordinate axes, we can write

$$M_x = -qM\sin\phi = -qMy/R_0,$$

$$M_y = qM\cos\phi = qMx/R_0.$$

Then, for the energy of interaction of a certain element with the remaining matrix, we obtain

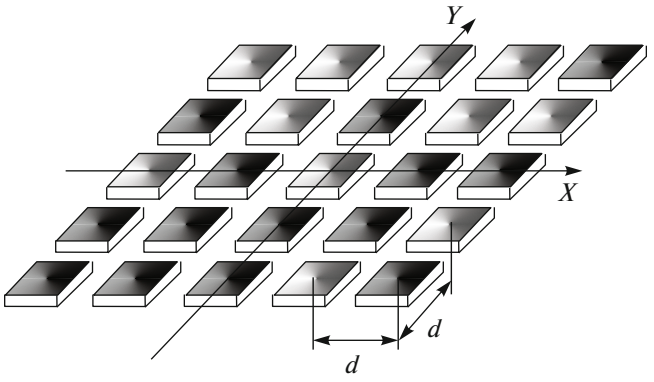

Fig. 5. Model for a two-dimensional array of square elements.

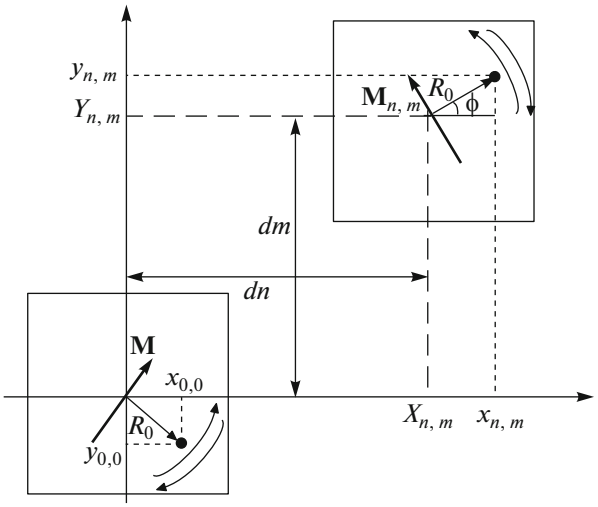

Fig. 6. Coordinate system and the scheme of the magnetostatic interaction between square elements. A heavy point indicates the position of the vortex core, and a heavy arrow, the direction of a magnetic moment. Both disks have the same chirality $q = 1$ (clockwise magnetization direction near the core). Thin arrows near the disk edges indicate possible core motion directions.

$$U_{\rm dip} = \frac{\mu_0}{4\pi}\frac{q_{0,0}M^2}{d^3R_0^2}\sum_{(n+m)\neq 0}\left(q_{n,m}\frac{y_{0,0}y_{n,m}+x_{0.0}x_{n,m}}{(n^2+m^2)^{3/2}}\right.$$
$$\left.-\frac{3q_{n,m}}{(n^2+m^2)^{5/2}}(-y_{0,0}n+x_{0,0}m)(-y_{n,m}n+x_{n,m}m)\right) \quad (11)$$
$$=\varepsilon\sum_{(n+m)\neq 0}\frac{q_{0,0}q_{n,m}}{(n^2+m^2)^{5/2}}\{x_{0,0}[x_{n,m}(n^2-2m^2)+3nmy_{n,m}]$$
$$+y_{0,0}[y_{n,m}(m^2-2n^2)+3nmx_{n,m}]\},$$

where R_0 is the root-mean-square radius of the vortex core trajectory and $\varepsilon = \mu_0 M^2/R_0^2 d^3$. It is important that the sign of π_T affects the direction of the effective magnetic moment of the disk when the core moves and the direction of core rotation about the center of the square (clockwise or counterclockwise) [31, 45].

The Zeeman energy of an element with indices $\{n, m\}$ can be written as

$$U_H = -\mathbf{M}_{n,m}[\mathbf{H}+\mathbf{h}_0(t)], \quad (12)$$

where $\mathbf{H} = H_z\mathbf{k} = hH_s\mathbf{k}$ is the dc magnetic field applied normal to the film surface. $\mathbf{h}_0(t) = h_0(t)\mathbf{j}$ is the small ac component of the applied field along axis y (unit vector $\mathbf{j}$). Then, allowing for Fig. 6, for energy U_H we have

$$U_H = U_0 - \mathbf{M}\cdot\mathbf{h}_0(t) = U_0 - \frac{q_{n,m}Mh_0(t)}{R_0}x_{n,m}. \quad (13)$$

Under steady core motion conditions, quantity $U_0 = -M_zH_z$ does not change in time and not depend on radius vector $\mathbf{r}$ of the core.

With allowance for Eqs. (11) and (13), we obtain the following system of equations for Eq. (1) in projections onto the coordinate axes (for brevity, indices {0, 0} are omitted):

$$-GV_y - DV_x - \kappa x + F_{{\rm dip}_x} + f_x = 0,$$
$$GV_x - DV_y - \kappa y + F_{{\rm dip}_y} = 0. \quad (14)$$

Here, we introduced the following designations:

$$F_{{\rm dip}_x} = -\frac{\partial U_{\rm dip}}{\partial x}$$
$$=-\varepsilon\sum_{n+m\neq 0}qq_{n,m}\left(\frac{n^2-2m^2}{(n^2+m^2)^{5/2}}x_{n,m}+\frac{3nm}{(n^2+m^2)^{5/2}}y_{n,m}\right), \quad (15)$$
$$F_{{\rm dip}_y} = -\frac{\partial U_{\rm dip}}{\partial y}$$
$$=-\varepsilon\sum_{n+m\neq 0}qq_{n,m}\left(\frac{m^2-2n^2}{(n^2+m^2)^{5/2}}y_{n,m}+\frac{3nm}{(n^2+m^2)^{5/2}}x_{n,m}\right),$$
$$f_x = -\frac{\partial U_H}{\partial x} = \frac{qM}{R_0}h_0(t),$$
$$V_x \equiv \frac{dx}{dt}, \quad V_y \equiv \frac{dy}{dt}.$$

For further calculations, we assume that the ac field component changes according to a harmonic law $h_0(t) = \eta\cos\omega t$ at cyclic frequency ω. We now solve the system of equations (14) in the form of traveling waves [9],

$$x_{n,m} = x_{0_{n,m}}\cos(-\omega_{n,m}t + \mathbf{K}\cdot\mathbf{r}_{n,m}),$$
$$y_{n,m} = y_{0_{n,m}}\sin(-\omega_{n,m}t + \mathbf{K}\cdot\mathbf{r}_{n,m}),$$

where $\mathbf{K}$ is the wavevector. The values of $\omega_{n,m}$ under steady conditions are the same in magnitude for different elements, and its sign (core precession direction) is determined by parameter π_T.

We now consider particular cases of the distribution of parameters p and q. Assume that only elements of two kinds with parameters $\{p_1, q_1\}$ and $\{p_2, q_2\}$ form a matrix and that they are symmetrically distributed with respect to axes x and y. For example, this distribution corresponds to staggered and banded structures, which will be considered below. The assumption of a symmetric distribution of the element parameters substantially simplifies the calculations of the sums in Eqs. (15).

As a result of the substitution of such calculations into Eq. (14), we obtain the following system for elements of both kinds:

$$G_1\omega y_{0_1} + (iD\omega+\kappa)x_{0_1}$$
$$=\frac{q_1M\eta}{R_0}e^{i\varphi_0} - \varepsilon x_{0_1}S_1^{(1)} - \varepsilon x_{0_2}q_1q_2S_1^{(2)},$$
$$G_1\omega x_{0_1} + (iD\omega+\kappa)y_{0_1} = -\varepsilon y_{0_1}S_2^{(1)} - \varepsilon y_{0_2}p_1p_2S_2^{(2)},$$
$$G_2\omega y_{0_2} + (iD\omega+\kappa)x_{0_2} \quad (16)$$
$$=\frac{q_2M\eta}{R_0}e^{i\varphi_0} - \varepsilon x_{0_2}S_1^{(1)} - \varepsilon x_{0_1}q_1q_2S_1^{(2)},$$
$$G_2\omega x_{0_2} + (iD\omega+\kappa)y_{0_2} = -\varepsilon y_{0_2}S_2^{(1)} - \varepsilon y_{0_1}p_1p_2S_2^{(2)}.$$

For the sums, we introduced the following designations:

$$S_1^{(1)} = \sum_{n+m\neq 0}\frac{n^2-2m^2}{(n^2+m^2)^{5/2}}\cos(K_xnd)\cos(K_ymd),$$
$$S_1^{(2)} = \sum_{n+m\neq 0}\frac{n^2-2m^2}{(n^2+m^2)^{5/2}}\cos(K_xnd)\cos(K_ymd),$$
$$S_2^{(1)} = \sum_{n+m\neq 0}\frac{m^2-2n^2}{(n^2+m^2)^{5/2}}\cos(K_xnd)\cos(K_ymd), \quad (17)$$
$$S_2^{(2)} = \sum_{n+m\neq 0}\frac{m^2-2n^2}{(n^2+m^2)^{5/2}}\cos(K_xnd)\cos(K_ymd).$$

The sums in Eqs. (17) should be taken according to the kind of element; that is, n and m should be indices for elements with the same combination of p and q. Thus, sums $S_1^{(1)}$ and $S_2^{(1)}$ are taken over the elements of the

first kind, and sums $S_1^{(2)}$ and $S_2^{(2)}$, over the elements of the second kind.

Using the system of equations (16), we can determine complex amplitudes $\{x_{0_1}, y_{0_1}, x_{0_2}, y_{0_2}\}$. The trajectory of a magnetic vortex core in a square element of the first kind is close to an elliptical trajectory with semiaxes $R_{0_x} = |x_{0_1}|$ and $R_{0_y} = |y_{0_1}|$, where

$$x_{0_1} = \frac{q_1 M\eta}{R_0 Z} e^{i\varphi_0}\{[(iD\omega + \kappa + \varepsilon S_2^{(1)})^2 - \varepsilon^2 S_2^{(2)^2}] \times (iD\omega + \kappa + \varepsilon S_1^{(1)} - \varepsilon S_1^{(2)}) + G_2^2\omega^2(iD\omega + \kappa + \varepsilon S_2^{(1)}) + G_1 G_2 \omega^2 \varepsilon S_2^{(2)}\}, \quad (18)$$

$$y_{0_1} = \frac{p_1 M\eta\omega}{R_0 Z} e^{i\varphi_0}\{[G_2\omega S_2^{(2)} - G_1(iD\omega + \kappa + \varepsilon S_2^{(1)})] \times (iD\omega + \kappa + \varepsilon S_1^{(1)} - \varepsilon S_1^{(2)}) + G_1 G_2^2 \omega^2\}.$$

Quantity Z has the form

$$Z = -G_1^2 G_2^2 \omega^4 + (iD\omega + \kappa + \varepsilon S_1^{(1)}) + (iD\omega + \kappa + \varepsilon S_2^{(1)})(G_1^2 + G_2^2)\omega^2 + 2G_1 G_2 \omega^2 \varepsilon^2 S_1^{(2)} S_2^{(2)} - [(iD\omega + \kappa + \varepsilon S_1^{(1)})^2 - \varepsilon^2 S_1^{(2)^2}] \times [(iD\omega + \kappa + \varepsilon S_2^{(1)})^2 - \varepsilon^2 S_2^{(2)^2}]. \quad (19)$$

Similarly, we can derive expressions for the core trajectory characteristics for an element of the second kind.

The resonance frequencies are determined by both the characteristics of individual magnets (G, κ, D) and the rigidity of a magnetostatic coupling, which is determined by ε and sums (17). It is important that the removal of degeneracy of frequencies with different combinations of polarities and chiralities is explained by the presence of terms having product $G_1 G_2$ raised to odd powers in Eqs. (18) and (19). In addition, the absolute values of parameters G, κ, and D depend on the perpendicular component of the magnetic field; therefore, its change leads to a change in the frequency and a displacement of a resonance peak.

We now consider a particular staggered distribution of the kinds of elements in an array. This distribution of the topological charge of elements is most often in a film [46]. Figure 7 shows possible combinations of p and q.

In the absence of an external field ($h = 0$), the absolute values of parameters G_1 and G_2 are the same; therefore, the distributions from Fig. 7 form two sets with different frequencies and each set is octuple-degenerate. For example, combinations with numerals {1, 4, 5, 8, 9, 12, 13, 16} have eigenfrequency ω_1 and set {2, 3, 6, 7, 10, 11, 14, 15} has eigenfrequency ω_2. The differences between the resonance frequencies in this case ensure different signs of chirality irrespective of the sign of polarity. When a field is applied ($h > 0$), the degeneracy of frequencies ω_1 and ω_2 is partly removed because of the dependence of parameters G and κ on the value and the sign of h. In this case, six sets, namely, {1, 4}, {2, 3}, {5, 8, 9, 12}, {6, 7, 10, 11}, {13, 16}, {14, 15}, give curves with eight resonance peaks. The mode frequencies can be determined from the extremum of the array-absorbed power, which can be estimated from the expression

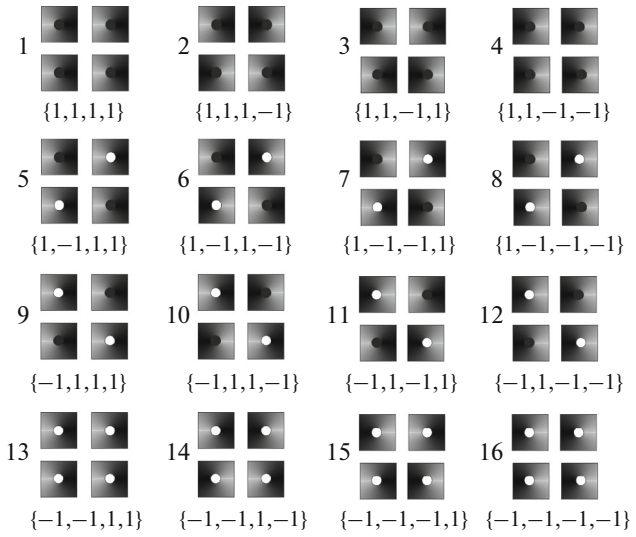

Fig. 7. Possible combinations of polarities and chiralities $\{p_1, p_2, q_1, q_2\}$ of arrays of elements of two kinds arranged in a staggered order. Elements with different chiralities have different contrasts. The direction of core polarity is indicated by black or white filling of the central region in a square.

$$P(\omega, h)_{\{p_1,p_2,q_1,q_2\}} = D\omega^2(|x_{0_1}|^2 + |y_{0_1}|^2 + |x_{0_2}|^2 + |y_{0_2}|^2). \quad (20)$$

Figure 8 shows the $P(\omega, h)$ curves obtained in the long-wavelength limit ($K_x = K_y = 0$) using Eq. (20) with allowance for Eqs. (18) and analogous expressions for x_{0_2} and y_{0_2}. At $K_x = K_y = 0$, from Eqs. (17) we have

$$S_1^{(1)} = S_2^{(1)} = -0.474, \quad S_1^{(2)} = S_2^{(2)} = -1.256.$$

As a consequence of pair equality of sums, the mode frequencies of sets {2, 3}, {5, 8, 9, 12} and {14, 15}, {5, 8, 9, 12} coincide. We used Eq. (10) to calculate the parameter of the quasi-elastic force coefficient.

We now consider another interesting case of the distribution of the kinds of element over an array, namely, a banded structure. The schematic of such a structure is shown in Fig. 9. We assume that parameters p and q are unchanged along axis y and alternate along x.

In this case, the calculation of power (20) differs from the previous calculation only in summation (17).

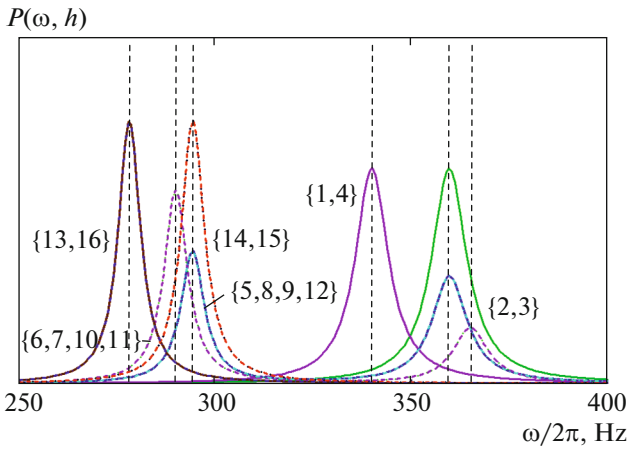

Fig. 8. (Color online) Resonance curves calculated by Eq. (20) for a staggered distribution of the kinds of elements at a magnetic field $h = 0.1$ and the center distance of squares $d = 5L$. Vertical dashed lines indicate resonance frequencies. p and q combination numbers are given in curly brackets at the curves according to Fig. 7.

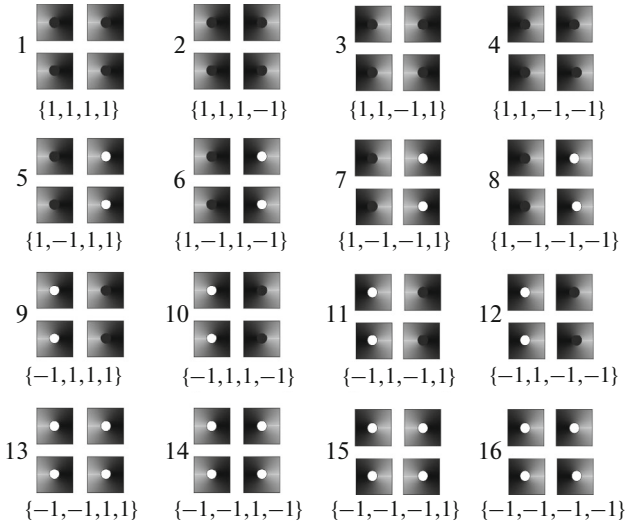

Fig. 9. Possible combinations of polarities and chiralities $\{p_1, p_2, q_1, q_2\}$ of elements of two kinds forming a banded structure.

As in the case of a staggered structure, we have eight resonance frequencies for sets with the same combinations of p and q in the presence of a magnetic field. Sums (17) for such a structure take the following values:

$$S_1^{(1)} = -2.328, \quad S_1^{(2)} = 0.599,$$

$$S_2^{(1)} = 1.051, \quad S_2^{(2)} = -2.371.$$

No coinciding resonance frequencies exist since $S_1^{(1)} \neq S_2^{(1)} \neq S_1^{(2)} \neq S_2^{(2)}$. Figure 10 shows resonance curves for a banded structure.

4. DISPERSION LAWS

It is difficult to perform an analytical calculation of the dependences of the mode frequencies on wavenumbers K_x and K_y in the general case with allowance for damping; therefore, we assume $D \ll G_1, G_2$ for simplicity. In this case, allowing for Eq. (19), we can write the following eigenfrequency equation:

$$\begin{aligned} &-G_1^2G_2^2\omega^4 + (\kappa + \varepsilon S_1^{(1)})(\kappa + \varepsilon S_2^{(1)})(G_1^2 + G_2^2)\omega^2 \\ &+ 2G_1G_2\omega^2\varepsilon^2 S_1^{(2)}S_2^{(2)} - [(\kappa + \varepsilon S_1^{(1)})^2 - \varepsilon^2 S_1^{(2)^2}] \\ &\times [(\kappa + \varepsilon S_2^{(1)})^2 - \varepsilon^2 S_2^{(2)^2}] = 0. \end{aligned} \quad (21)$$

The solution to this biquadratic equation is

$$\omega_{1,2}^2 = A \pm \sqrt{A^2 - B}, \quad (22)$$

where

$$\begin{aligned} A &= \frac{1}{2G_1^2G_2^2}\left[(G_1^2 + G_2^2)(\kappa + \varepsilon S_1^{(1)})(\kappa + \varepsilon S_2^{(1)}) + 2G_1G_2\varepsilon^2 S_1^{(2)}S_2^{(2)}\right], \\ B &= \frac{1}{G_1^2G_2^2}((\kappa + \varepsilon S_1^{(1)})^2 - \varepsilon^2 S_1^{(2)^2})((\kappa + \varepsilon S_2^{(1)})^2 - \varepsilon^2 S_2^{(2)^2}). \end{aligned} \quad (23)$$

The following simple particular cases are of interest. In the absence of interaction between magnetic elements, Eq. (22) takes the form

$$\omega_{1,2}^2 = \frac{\kappa^2}{2G_1^2G_2^2}[(G_1^2 + G_2^2) \pm (G_1^2 - G_2^2)]. \quad (24)$$

Frequencies (24) correspond to the well-known result for the motion of cores in two independent elements with different values of gyrovectors.

Another useful case corresponds to the absence of an applied magnetic field ($h = 0$). In this case, we have $|G_1| = |G_2| = G$ and, from Eq. (22), for the frequencies obtain

$$\begin{aligned} \omega_1^2 &= \frac{1}{G^2}(\kappa + \varepsilon S_1^{(1)} + \varepsilon S_1^{(2)})(\kappa + \varepsilon S_2^{(1)} + \varepsilon S_2^{(2)}), \\ &q_1 = q_2, \\ \omega_2^2 &= \frac{1}{G^2}(\kappa + \varepsilon S_1^{(1)} + \varepsilon S_1^{(2)})(\kappa + \varepsilon S_2^{(1)} - \varepsilon S_2^{(2)}), \\ &q_1 = -q_2. \end{aligned} \quad (25)$$

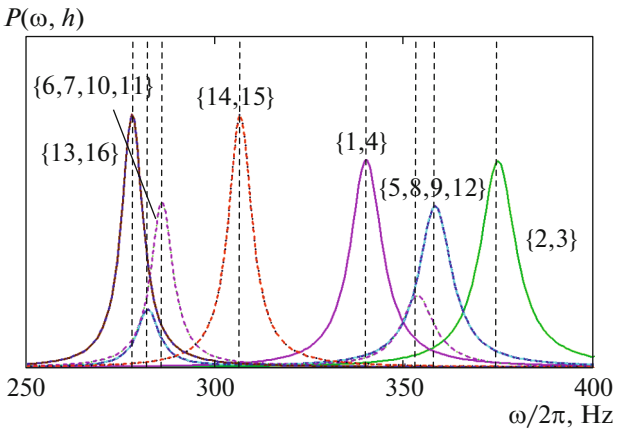

Fig. 10. (Color online) Resonance curves calculated by Eq. (20) for a banded structure at a magnetic field $h = 0.1$ and the center distance of squares $d = 5L$. Vertical dashed lines indicate resonance frequencies.

Here, we have the frequencies of two modes corresponding to core rotation in one direction (ω_1) and in opposite directions (ω_2).

Let us return to the general case $h \neq 0$ ($G_1 \neq G_2$). The eigenfrequencies of the corresponding modes are determined from the extremum of the absorbed power,

$$\frac{\partial}{\partial\omega} P(\omega, h)_{\{p_1,p_2,q_1,q_2\}} = 0.$$

This condition allows us to find dispersion laws $\omega(K_x, K_y)_{\{p_1,p_2,q_1,q_2\}}$, which are shown in Fig. 11.

In conclusion of this section, we note that, in principle, modern experimental facilities can be used to excite and detect short-wavelength modes and, hence, to study $\omega(K_x, K_y)$ dependences in arrays of ferromagnetic nano- and microelements [11].

5. EXPERIMENT

Arrays of square nanodots were formed by lift-off lithography from a continuous film using high-vacuum thermal deposition of an 80NKhS alloy onto a photoresist-coated silicon wafer. A negative AZ Nlof 2035 photoresist was used to create the required surface morphology of the substrate. To observe the mag-

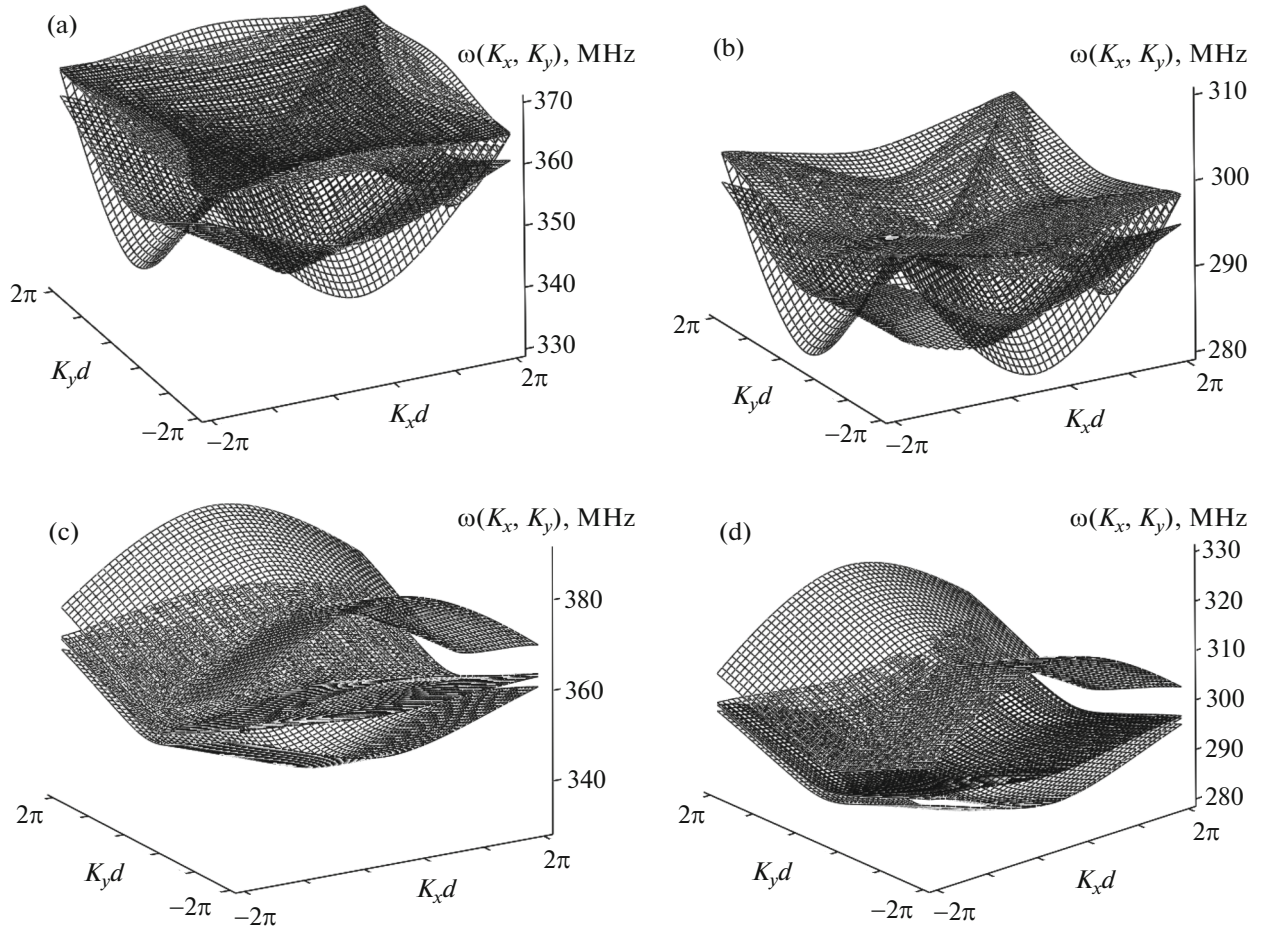

Fig. 11. Dispersion surfaces for (a, b) staggered and (c, d) banded structures. For convenience, the high- and low-frequency ranges are separated. The surface were plotted at $h = 0.1$.

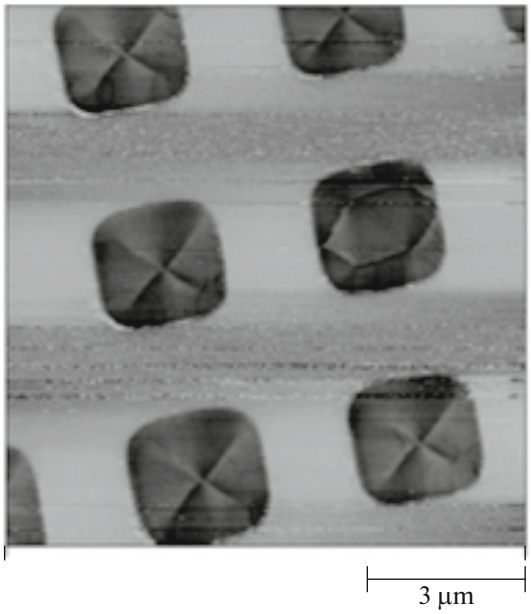

Fig. 12. Atomic force microscopy image of the magnetization structure in part of the array of square elements.

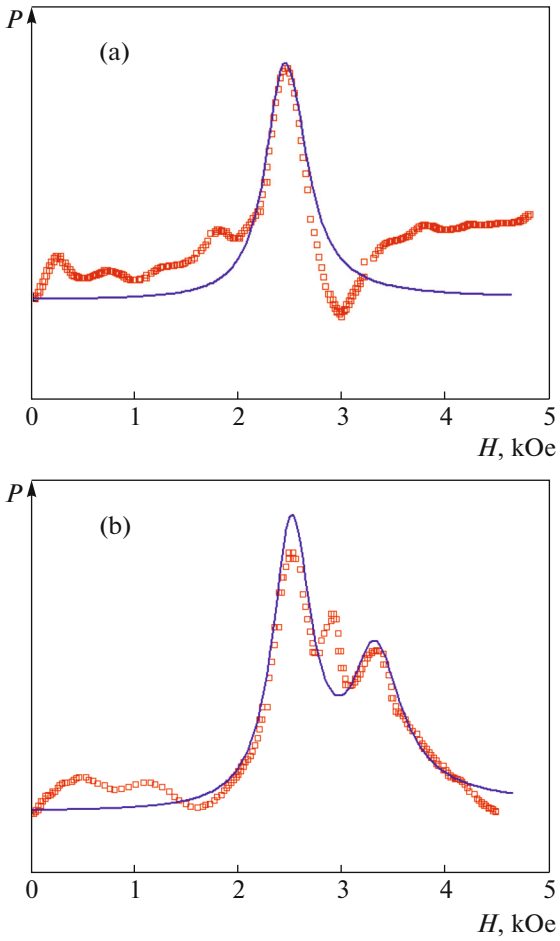

Fig. 13. (Color online) (circles) Integrated power absorption curves obtained from experimental data in comparison with (solid curves) calculated absorption power for arrays with the center distance of elements of (a) 9 and (b) 5 μm.

netic structure of ferromagnetic nanospots, we applied a Veeco MultiMode NanoScope IIIa SPM System scanning probe force microscope. Figure 12 depicts a characteristic scan of the magnetic structure, which was taken according to a two-pass technique under cantilever frequency modulation. The reverse pass height was $z_0 = 50$ nm. These images allow the conclusion that an equilibrium structure with a closed magnetic flux (quasi-vortex) of four domains separated by 90° Néel boundaries most often forms in square elements. A core, which is similar to that formed at the center of circular elements, is located at the center of a square, at the intersection of diagonals.

The resonance behavior of magnetization was studied on an FMR spectrometer. A sample was placed at the antinode of a high-frequency magnetic field of frequency $\omega = 415$ MHz. The in-plane ac magnetic field amplitude was 1 Oe. The field was normal to the waveguide plane. A signal from the sample was amplified by a selective amplifier at a modulation frequency of 1 kHz and was transferred to a synchronous detector. Applied magnetic field H was changed in the range 0–5 kOe. The square element thickness was about 12 nm.

It should be noted that we could not control chirality during sample preparation; therefore, we expected that parameter q in an array of elements was randomly distributed. However, force microscopy showed that the film was actually divided into islands, i.e., families of neighboring elements with the same chirality. The number of element in the islands is random and varied over wide limits; on average, it is about ten. The chiralities of the elements belonging to neighboring islands and located at their boundaries are opposite. Thus, a variety of structures with various combinations of parameters $\{p, q\}$ takes place in the array of particles. Note that the same value of polarity p can be ensured by magnetizing the film to saturation in the direction normal to the surface under resonance conditions.

As a result of the experiment, we obtained absorption curves, the integrated shape of which is shown as dots in Fig. 13. The solid line illustrates the theoretical dependence obtained by the summation of Eq. (20) over various combinations of polarity and chirality for a staggered structure taken as the most general case. The calculation was performed in the long-wavelength limit ($K_x = K_y = 0$) by summation over all possible combinations of parameters p and q with weighting factors as adjustable parameters.

As is seen in Fig. 13, one absorption peak exists at large distances between array elements, when the mutual influence is negligible. This peak corresponds

to the resonance motion of vortex cores in the elements where the combination of the signs of polarity and chirality turned out to be favorable for a given direction and magnitude of a magnetic field. At small distances between elements, the interaction between them causes coupled core motion, and different oscillation modes are excited at different fields for certain combinations of polarity and chirality. As a result, we observe a set of resonance frequencies. Since no direct contact or magnetic bridges between elements are observed, it is reasonable to assume that the magnetizations interact via magnetostatics.

6. CONCLUSIONS

In the model of noninteracting elements, only the elements that have a favorable core polarity would exhibit resonance behavior of magnetization. Only one resonance frequency is fixed in this case. At a generator frequency $\omega > \omega_0$, the polarity direction along an applied magnetic field is favorable (ω_0 is the core frequency in an isolated element in the absence of a magnetic field). At $\omega < \omega_0$, a resonance is fixed when polarity is opposite to the field direction [8]. The collective motion of cores in normal modes can occur in the presence of an interaction between the magnetic subsystems of the elements. Such modes are excited when elements with a favorable polarity direction exist in an array.

Satisfactory qualitative agreement between the experimental data and the analytical estimates suggests that the assumption regarding a magnetostatic origin of the splitting of the FMR frequency is correct (see Fig. 13). The normal mode frequencies of magnetization oscillation differ weakly from the resonance frequency of core motion in an individual element at a large distance between array elements because of the weakness of their interaction. In this case, power absorption curves are superimposed to form only one clear maximum. When the distance between the elements in an array decreases, the coupling between the magnetic moments of the elements becomes substantial, and the differences between the normal mode frequencies are so high that individual peaks in absorption curves appear.

The quantitative discrepancy between the calculation by Eq. (20) and the experimental data can be explained by the following factors: a neglected magnetostatic interaction between the magnetic moments of the cores, noncylindrical symmetry of the potential in which a core is located as a quasiparticle, and the error related to the application of the rigid vortex model. In addition, the following interesting factors are operative: (a) a quadrupole term is to be taken into account in the calculation of the magnetostatic interaction energy of noncircular elements [47]; (b) the shape of elements causes anisotropy in the film plane, and the axis direction can change as a function of the element–element distance [48]. It should be noted that these factors introduce quantitative corrections and do not change the general picture of removing frequency degeneracy.

In conclusion, we note that the mutual effect of elements can be an obstacle to the attempts to find a reliable method for controlling the state of magnetization (polarity, chirality) in arrays of close-packed elements, which is important for spintronic devices. This factor is especially important at the magnetic field frequencies that are close to eigenfrequencies. However, this factor opens up fresh opportunities for almost simultaneous control of the state of the set of elements involved in one oscillation mode. In any case, when designing devices based on large arrays of nano- and microelements, researchers have to take into account the mutual influence of their magnetic subsystems.

ACKNOWLEDGMENTS

This work is dedicated to cherished memory of P.D. Kim, who was an inspirer, an organizer, an idea man, and an example for the entire scientific team.

This work was supported by the Russian Foundation for Basic Research, project nos. 16-32-00103 and, in part, 18-02-00161.

REFERENCES

1. A. Thiele, Phys. Rev. Lett. **30**, 230 (1973).
2. B. A. Ivanov, G. G. Avanesyan, A. V. Khvalkovskiy, N. E. Kulagin, K. E. Zaspel, and K. A. Zvezdin, JETP Lett. **91**, 178 (2010).
3. J. Kim and S.-B. Choe, J. Magn. **12**, 113 (2007).
4. A. Puzic, B. Van Waeyenberge, K. W. Chou, P. Fischer, H. Stoll, G. Schutz, T. Tyliszczak, K. Rott, H. Bruckl, G. Reiss, I. Neudecker, Th. Haug, M. Buess, and C. H. Back, J. Appl. Phys. **97**, 10E704 (2005).
5. B. Pigeau, G. de Loubens, O. Klein, A. Riegler, F. Lochner, G. Schmidt, L. W. Molenkamp, V. S. Tiberkevich, and A. N. Slavin, Appl. Phys. Lett. **96**, 132506 (2010).
6. K. Yu. Guslienko, V. Novosad, Y. Otani, H. Shima, and K. Fukamichi, Phys. Rev. B **65**, 024414 (2001).
7. S. N. Vdovichev, B. A. Gribkov, S. A. Gusev, V. L. Mironov, D. S. Nikitushkin, A. A. Fraerman, and V. B. Shevtsov, Phys. Solid State **48**, 1902 (2006).
8. G. Loubens, A. Riegler, B. Pigeau, F. Lochner, F. Boust, K. Y. Guslienko, H. Hurdequint, L. W. Molekamp, G. Schmidt, A. N. Slavin, S. Tiberkevich, N. Vukadinovic, and O. Klein, Phys. Rev. Lett. **102**, 177602 (2009).
9. P. D. Kim, V. A. Orlov, R. Yu. Rudenko, V. S. Prokopenko, I. N. Orlova, and A. V. Kobyakov, J. Magn. Magn. Mater. **440**, 171 (2017).
10. V. S. Prokopenko, P. D. Kim, V. A. Orlov, B. V. Vasiliev, D. K. Vovk, S. E. Zatsepilin, and R. Yu. Rudenko, J. Siber. Fed. Univ. Math. Phys. **6**, 262 (2013).

11. S. Erokhin and D. Berkov, Phys. Rev. B **89**, 144421 (2014).
12. B. VanWaeyenberge, A. Puzic, H. Stoll, K. W. Chou, T. Tyliszczak, R. Hertel, M. Fahnle, H. Bruckl, K. Rott, G. Reiss, I. Neudecer, D. Weiss, C. H. Back, and G. Schutz, Nat. Lett. **444**, 461 (2006).
13. A. Vogel, T. Kamionka, M. Martens, A. Drews, K.-W. Chou, T. Tyliszczak, H. Stoll, B. VanWaeyenberge, and G. Meier, Phys. Rev. Lett. **106**, 137201 (2011).
14. S.-B. Choe, Y. Acremann, A. Scholl, A. Bauer, A. Doran, J. Stohr, and H. A. Padmore, Science (Washington, DC, U. S.) **304**, 420 (2004).
15. F. Peng and D. Hui, Ann. Phys. **523**, 417 (2011).
16. M. Konoto, T. Yamada, K. Koike, H. Akoh, T. Arima, and Y. Tokura, J. Appl. Phys. **103**, 023904 (2008).
17. Yu. I. Gorobets, Yu. I. Dzhezherya, and A. F. Kravets, Phys. Solid State **42**, 126 (2000).
18. J. Dou, S. C. Hernandez, Ch. Yu, M. J. Pechan, L. Folks, J. A. Katine, and M. J. Carey, J. Appl. Phys. 107, 09B514 (2010).
19. A. Yu. Galkin and B. A. Ivanov, and C. E. Zaspel, Phys. Rev. B **74**, 144419 (2006).
20. A. Yu. Galkin and B. A. Ivanov, J. Exp. Theor. Phys. **109**, 74 (2009).
21. J. Shibata and Y. Otani, Phys. Rev. B **70**, 012404 (2004).
22. P. D. Kim, V. A. Orlov, R. Yu. Rudenko, V. S. Prokopenko, I. N. Orlova, and S. S. Zamai, JETP Lett. **101**, 562 (2015).
23. H. Jung, Y.-S. Yu, Ki-Suk Lee, Mi-Young Im, P. Fischer, L. Bocklage, A. Vogel, M. Bolte, G. Meier, and S.-K. Kim, Appl. Phys. Lett. **97**, 222502 (2010).
24. Ki-Suk Lee, H. Jung, D.-S. Han, and S.-K. Kim, J. Appl. Phys. **110**, 113903 (2011).
25. D.-S. Han, A. Vogel, H. Jung, Ki-Suk Lee, M. Weigand, H. Stoll, G. Schutz, P. Fischer, G. Meier, and S.-K. Kim, Sci. Rep. **3**, 2262 (2013). doi 10.1038/srep02262
26. O. Klein, G. de Loubens, V. V. Naletov, F. Boust, T. Guillet, H. Hurdequint, A. Leksikov, A. N. Slavin, V. S. Tiberkevich, and N. Vukadinovic, Phys. Rev. B **78**, 144410 (2008).
27. K.-S. Lee and S.-K. Kim, Appl. Phys. Lett. **91**, 132511 (2007).
28. V. P. Kravchuk, Yu. Gaididei, and D. D. Sheka, Phys. Rev. B **80**, 100405(R) (2009).
29. K.-S. Lee, K. Yu. Guslienko, J.-Y. Lee, and S.-K. Kim, Phys. Rev. B **76**, 174410 (2007).
30. B. A. Ivanov and G. M. Wysin, Phys. Rev. B **65**, 134434 (2002).
31. K. Yu. Guslienko, B. A. Ivanov, V. Novosad, Y. Otani, H. Shima, and K. Fukamichi, J. Appl. Phys. **91**, 8037 (2002).
32. J. P. Park, P. Eames, D. M. Engebretson, J. Berezovsky, and P. A. Crowell, Phys. Rev. B 67, 020403(R) (2003).
33. B. A. Ivanov, E. G. Galkina, and A. Yu. Galkin, J. Low Temp. Phys. **36**, 747 (2010).
34. A. K. Zvezdin and K. A. Zvezdin, J. Low Temp. Phys. **36**, 826 (2010).
35. R. G. Elrias and A. D. Verga, Phys. Rev. B **89**, 134405 (2014).
36. S. S. Cherepov, B. C. Koop, V. Korenivski, D. C. Worledge, A. Yu. Galkin, R. S. Khymyn, and B. A. Ivanov, Phys. Rev. Lett. **109**, 097204 (2012).
37. K. Yu. Guslienko, X. F. Han, D. J. Keavney, R. Divan, and S. D. Bader, Phys. Rev. Lett. **96**, 067205 (2006).
38. M. Wolf, U. K. Robler, and R. Schafer, J. Magn. Magn. Mater. **314**, 105 (2007).
39. E. G. Galkina, B. A. Ivanov, and V. A. Stephanovich, J. Magn. Magn. Mater. **118**, 373 (1993).
40. P. D. Kim, V. A. Orlov, V. S. Prokopenko, S. S. Zamai, V. Ya. Prints, R. Yu. Rudenko, and T. V. Rudenko, Phys. Solid State **57**, 30 (2015).
41. A. D. Belanovsky, N. Locatelli, P. N. Skirdkov, F. Abreu Araujo, J. Grollier, K. A. Zvezdin, V. Cros, and A. K. Zvezdin, Phys. Rev. B **85**, 100409(R) (2012).
42. B. A. Ivanov and C. E. Zaspel, Phys. Rev. Lett. **99**, 247208 (2007).
43. A. Vogel, A. Drews, T. Kamionka, M. Bolte, and G. Meier, Phys. Rev. Lett. **105**, 037201 (2010).
44. J. Shibata, K. Shigeto, and Yo. Otani, Phys. Rev. B **67**, 224404 (2003).
45. F. G. Mertens and A. R. Bishop, arXiv: cond-mat/9903037v1.
46. A. Yu. Galkin, B. A. Ivanov, and A. Yu. Merkulov, J. Exp. Theor. Phys. **101**, 1106 (2005).
47. C. Phatak, R. Pokharel, M. Beleggia, and M. de Graef, J. Magn. Magn. Mater. **323**, 2912 (2011).
48. Li Sun, Xiao Zou, Wen Zhang, Guodong Li, Ya Zhai, Jing Wu, Yongbing Xu, and Hongru Zhai, Phys. Status Solidi C **9**, 66 (2012).

Translated by K. Shakhlevich